Journal of the Brazilian Society of Mechanical Sciences and Engineering (2019) 41:230
https://doi.org/10.1007/s40430-019-1730-y

TECHNICAL PAPER

A novel creep test rig to study the effects of long-range residual stress, elastic follow-up and applied load

A. M. Shirahatti[1] · **D. J. Smith**[2]

Received: 10 September 2018 / Accepted: 10 April 2019 / Published online: 20 April 2019

Abstract

One of the many challenges in the behaviour of structures is to understand if the presence of residual stress plays an important role in contributing to failure of a structure operating at high temperature. Assessments of the high-temperature integrity of practical structures are based on experiments carried out using standard laboratory-scale creep test specimens tested under either load- or displacement-controlled conditions. In practice, structures are subjected to combinations of residual and applied stresses which in turn lead to mixed boundary conditions. Conventional laboratory creep tests do not represent these circumstances. The purpose of this paper is to describe the design of a novel test rig to introduce long-range residual stresses at high temperature. The concept of rig is based on three-bar structure with an initial misfit introduced into the central bar to represent a long-range residual stress and could be characterised easily without using time-consuming residual stress measurement techniques. Initial results demonstrated that the magnitude and the interaction of the residual stress with the applied loading is a function of the initial misfit displacements and the relative stiffness of the components of the system. Additionally, the subsequent behaviour of the system, with and without the application of additional loading, is governed by (a) the degree to which the misfit is accommodated by plastic and creep strain and (b) the elastic follow-up provided by the system. The paper describes the design of a test rig and laboratory tests conducted to validate the concept.

Keywords Creep · Elastic follow-up · Residual stress · 316H stainless steel

List of symbols

K_{in}	Middle bar stiffness other than specimen
K_{out}	Side bar stiffness
K_s	C(T) specimen stiffness
Z_{eff}	Elastic follow-up for bars in parallel
Z	Overall elastic follow-up
σ_{ref}	Reference stress
P	Applied load
E	Young's modulus of material
a_0	Initial crack length of C(T) specimen
B	Gross section thickness of C(T) specimen
B_n	Net section thickness of C(T) specimen
W	Width of C(T) specimen

Technical Editor: Paulo de Tarso Rocha de Mendonça, Ph.D.

✉ A. M. Shirahatti
anilshirahatti@gmail.com

[1] Department of Mechanical Engineering, Jain College of Engineering, Belagavi, India

[2] Solid Mechanics Group, Department of Mechanical Engineering, University of Bristol, Bristol BS8 1TR, UK

1 Introduction

Residual stress plays an important role in the component life assessment of the structures. Such stresses may arise usually as a consequence of the manufacturing process and final fabrication [1]. For accurate safety assessments, understanding how residual stresses interact with applied service loads is required as tensile residual stresses present in the components can combine with in-service loads to promote failure at a load which was viewed as safe. Residual stresses are usually treated as secondary stresses. However, in certain circumstances, they must be classed as primary. For example, in a cracked structure where the fit-up residual stresses do not self-equilibrate across a ligament, the residual stresses may provide a significant contribution to the plastic collapse of the ligament. Whether they do or not depends on how the residual forces change as a crack grows and plastic deformation accumulates in the structure. This in turn depends on the level of elastic follow-up (EFU). A typical practical case where we expect to see the effect of EFU is shown in Fig. 1 for a pressurised piping system. As shown schematically, the system and its welds can be treated as a series of

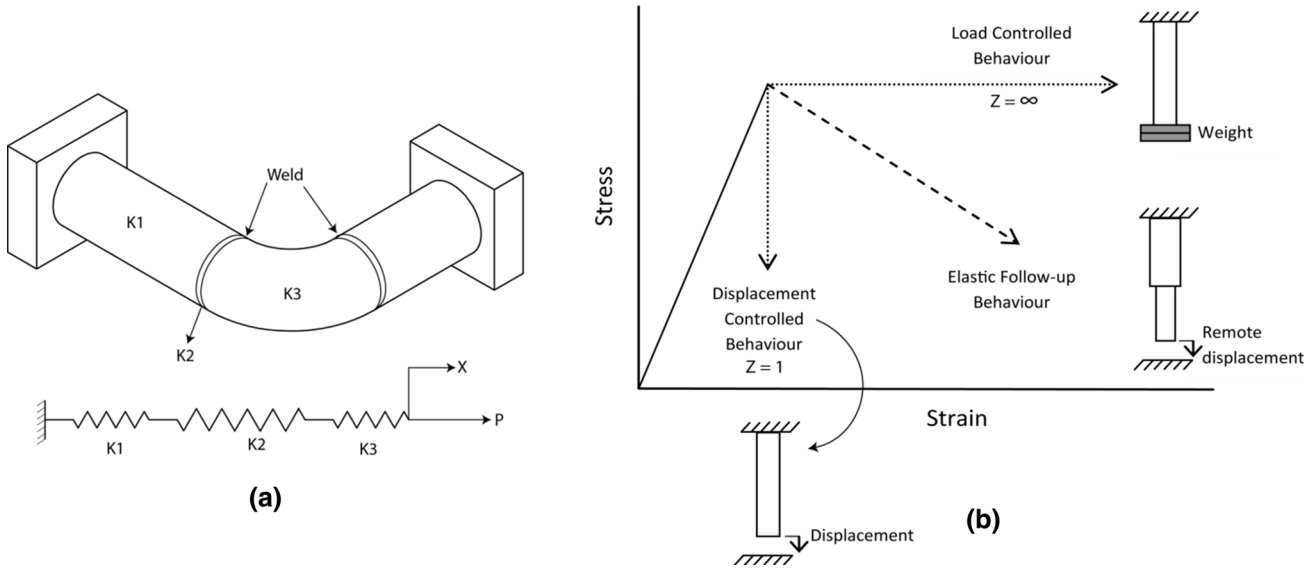

Fig. 1 **a** Built-in welded pipe bend (*P* is load and *X* is displacement), **b** stress–strain behaviour of a local volume

springs with the pipe having stiffness K1, K3 and the weld with stiffness K2. When the pipe is built-in and welded, we would expect long-range residual stresses to be present and those are represented as an initial far-field displacement *X*. The pipe will also be subjected to internal pressure, and consequently, the system is also subjected to external load P. Elastic follow-up is expected when part of a structure (the area around the welds) reduces its stiffness (either through creation of plasticity and/or the growth of crack) relative (i.e. EFU) to the surrounding material. This would result in additional strain accumulation and relaxation of the initial stresses created during the welding and fit-up.

Many methods have been proposed to generate well-defined residual stress fields in laboratory test specimens [2]. In the context of investigating the influence of residual stress on creep, the following methods have been developed: pre-compression [3–7], quenching [8], side punching [9], Borland specimens [10], ring weld specimens [11] and electron beam (EB) welding [1, 12, 13]. These methods produce either long-range or short-range residual stress fields. Quenching, Borland specimens and ring welding methods result in specimens with a residual stress field throughout the entire volume. On the other hand, side punching, in-plane compression and EB welding methods result in a residual stress field being set up in a much localised part of the specimen. The second group of methods rely on local, rather than global, incompatible displacements to set up the residual stress field.

Another important observation is that the in-plane compression and EB welded specimens require the introduction of a sharp notch by, for example, electro-discharge machining, prior to creep testing. Introducing such a notch redistributes the residual stresses, so care must be taken to ensure that the required levels of residual stress remain in the specimen after this redistribution. Consider the in-plane compression method as an example. Here, a volume of material local to the semicircular stress raiser deforms plastically and this plastic zone resists the relaxation of the surrounding material. If a long notch is introduced such that it extends through the plastic zone and into the surrounding elastic zone, then the elastic zone is free to relax and the residual stress field is lost [12].

In all the above methods, the magnitude and distribution of residual stress are found by time-consuming methods, i.e. neutron diffraction. Also, in all the cases, various nominally identical specimens are manufactured to determine the stress distribution. For example in case of cylinder quenching by Hossain [8], three specimens were manufactured and the neutron diffraction method was used to measure the stress distribution after quenching, short-term ageing (1.25 h) and long-term ageing (1800 h). In all of the above methods, residual stress is introduced at room temperature, and when the specimen is subjected to high temperature, the magnitude of residual stress is reduced drastically ($\approx 30\%$ reduction) [3–13] due to the lower yield strength at high temperature. In all the cases, the residual stress at high temperature was determined using finite element analysis.

In order to study the effect of residual stress, it is desirable that the method chosen to induce residual stress in the specimen causes no other changes which might influence creep. It is also desirable that residual stress fields set up in the laboratory creep specimens are representative of the long-range residual stress fields found in engineering structures.

Of the various methods reviewed, only side punching, in-plane compression and EB welding have been used to study the effect of residual stress and applied load on creep under load control conditions. These techniques can also be used to carry out displacement-controlled tests. In practical circumstances, relaxation of residual stress in one section is compensated by changes in residual stress distribution in other sections to keep the complete structure in equilibrium, i.e. components are often subjected to combined displacement and load-controlled situations as shown in Fig. 1b. Furthermore, it is now known [14] that depending on the stiffness of the structure, relaxation of the residual stress can be associated with elastic follow-up. However, none of the methods are amenable to measuring and monitoring accurately the residual stresses. Also there is no evidence in earlier experiments to indicate that the elastic follow-up has been measured or taken into account. The concept of elastic follow-up was introduced by Robinson [16] in connection with creep stress relaxation and has been developed further by others [14–19]. Most of the research uses two bar models to study the effect of elastic follow-up on creep, but this represents only a displacement boundary condition, whereas in practice, combinations of residual and applied stress lead to a mixed boundary condition in regions of interest in a structure.

The purpose of this paper is to illustrate a novel creep test rig that was designed to study the effect of elastic follow-up, long-range residual stress and applied load. A new method is presented that introduces residual stress in a controlled manner such that the stress can be calculated easily at any time and without the use of time-consuming residual stress measurement techniques. A preliminary series of tests have been completed to validate the behaviour of the test rig to carry out long-term creep tests under the influence of residual stress, elastic follow-up and combined load.

2 Test rig design

2.1 Concept of three-bar model

The new method is based on a classical three-bar model and is developed to introduce long-range residual stresses through strain incompatibility. This model (or system) has several key features relevant to the high-temperature problems of creep. The magnitude and the interaction of the residual stress with the applied loading are a function of the initial misfit displacements and the relative stiffness of the components of the system. The subsequent behaviour of the system, with and without the application of additional loading, is governed (a) by the degree to which the misfit is accommodated by plastic and creep strain and (b) the elastic follow-up provided by the system.

Figure 2 shows the three-bar structure model consisting of two side bars 'B' and a middle bar combination of bar 'A' and a creep specimen. The bars A and B are able to deform elastically and have stiffness K_{in} and K_{out}, respectively. An initial misfit 'X' exists between the bars so that joining the bars together introduces fit-up residual stresses into the system, with tension in bar A and balancing compression in bar B. The residual force in the middle bar does not self-equilibrate across a section, but the tensile residual force in middle bar is in equilibrium with the net compressive force in the outer bars. The structure can be subjected to the applied load 'P' so that when plasticity, creep or crack growth occurs in the specimen, the overall EFU factor Z is given by

$$Z = Z_{\text{eff}} Z_{\text{s}}, \tag{1}$$

where

$$Z_{\text{eff}} = \left(\frac{1+\alpha_{\text{eff}}}{\alpha_{\text{eff}}}\right) \text{ and } Z_{\text{s}} = \left(\frac{1+\beta}{\beta}\right)$$

$$\beta = \frac{K_{\text{in}}}{K_{\text{s}}}, \quad \frac{1}{K_{\text{eff}}} = \frac{1}{K_{\text{S}}} + \frac{1}{K_{\text{in}}}, \quad \alpha_{\text{eff}} = \frac{2K_{\text{out}}}{K_{\text{eff}}}, \tag{2}$$

and K_{s} is the stiffness of the specimen.

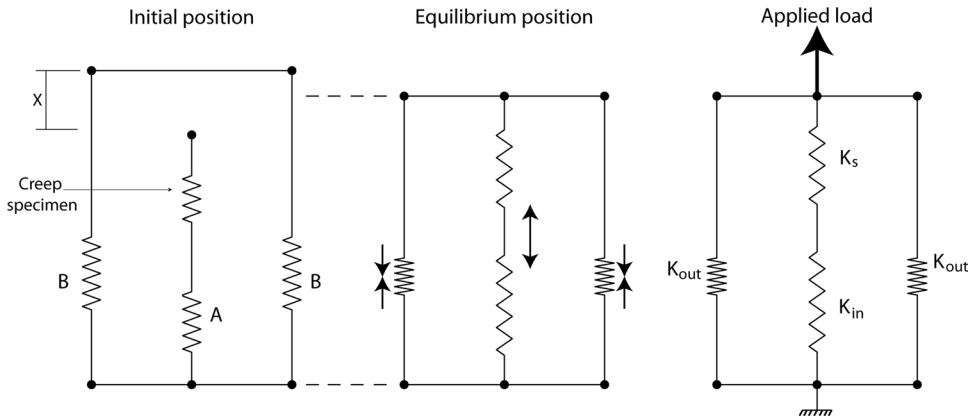

Fig. 2 Three-bar structure model

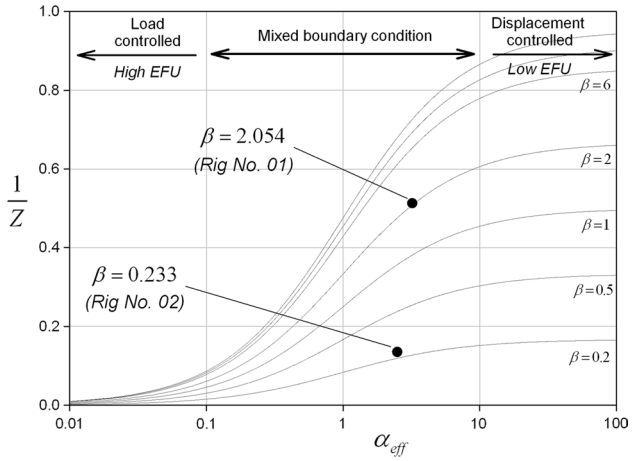

Fig. 3 Variation of overall EFU with effective stiffness ratio in three-bar structure

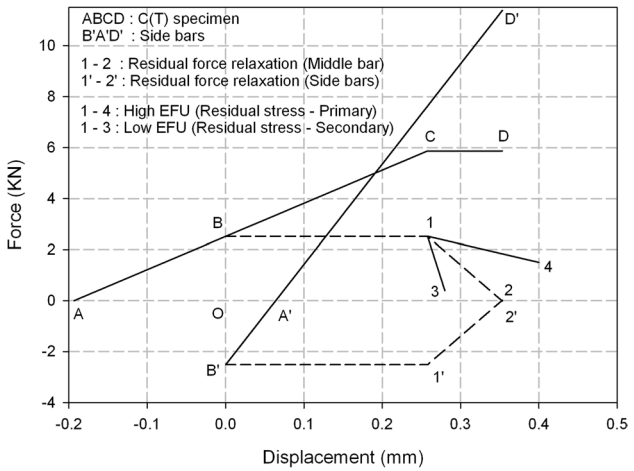

Fig. 4 Loading and subsequent relaxation of a three bar

A detailed derivation of this is given in [15]. Figure 3 shows the overall elastic follow-up factor as a function of relative effective stiffness ratio. When the elastic follow-up factor is in excess of 6 (or $1/Z = 0.167$), these conditions essentially correspond to load-controlled conditions, whereas an elastic follow-up factor of more than 1.25 (or $1/Z = 0.8$) represents displacement-controlled conditions.

2.2 Behaviour of the structure with applied load

Figure 4 shows loading conditions and relaxation during plasticity for a representative three-bar structure. AA′ gives the initial misfit; OB and OB′ give the residual force in middle and side bars, respectively. When the structure is further subjected to external load, the force in the middle bar increases from B to C. At point C, yielding of specimen starts and the specimen takes no further load and follows line CD, while outer bar remains in the elastic range and follows path A′D′. Until yielding at point C, the initially induced residual force remains constant in the middle and outer bars and follows paths B-1 and B′1′, respectively. As the applied load increases and the amount of plastic deformation in the specimen becomes equal to the initial misfit, the residual force reduces to zero. The rate of residual force relaxation for a mixed boundary condition follows path 1–2. The gradient of relaxation curves (1–3, 1–2 or 1–4) depends upon the elastic follow-up factor. Structures having high EFU will follow path 1–4, while low EFU structures will follow path 1–3. Hence, the influence of initial residual stress present in a structure is dependent on the associated level of EFU.

2.3 Design of creep test rig

In R5 [20], high-temperature assessment procedure, the difficulty of treating EFU by most design codes is discussed. Currently in integrity assessment procedures for cracked structures, no unified approach is available for incorporating the effects of EFU. The elastic follow-up factor for the uncracked body can be evaluated using the methods given in R5 Volume 2/3. In R5, it is suggested to increase the EFU factor calculated for the uncracked components by unity to allow for the additional follow-up due to presence of crack. For example, $Z = 1$ is for an uncracked tensile specimen and a value of $Z = 2$ is recommended for a C(T) specimen to accommodate additional follow-up that occurs in cracked components due to the difference between elastic and creep compliances. In cases where the EFU is high (say $Z > 5$), it is advised to treat the problem as load controlled ($Z = \infty$). The methods for determination of Z in R5 are based on judgment and experience. Extension of these procedures to cracked structures and cases where significant localised plasticity and crack growth introduce elastic follow-up remains to be addressed experimentally [14]. Hence, it is decided to construct two rigs with different EFU.

Two experimental test rigs with different elastic follow-up values were designed using three-bar concept, rig 1 to provide Z equal to about 2 and rig 2 with Z equal to 6. Since the design was centred around using a conventional cylindrical furnace with a maximum internal diameter of 130 mm within a creep test frame, the design was constrained to the available maximum diameter of the furnace, the overall length of the structure (1000 mm), ease of assembly, the ability to introduce known residual stress at high temperature and then to apply a predetermined load to the assembly. The overall arrangement of the test rig is shown in Fig. 5, and the material properties of the components for the test rig are given in Table 1. Overall the test rigs were designed to subject uniaxial or C(T) specimens to 550 °C. In present paper, C(T) specimens were used for design and analysis.

The middle bar was a combination of a 316H stainless steel C(T) specimen and a Nimonic (80A) bar, while the

outer bars were also Nimonic (80A) bars. The chemical composition of the Type 316H stainless steel is shown in Table 2. The overall heights of rig 1 and 2 were 740 and 865 mm, respectively. All bars were screwed to top and bottom end pieces made from EN24T steel. Two linear voltage displacement transducers (LVDT) were mounted on each side of the upper and lower ends to measure the total displacement of the structure. Also, a capacitance

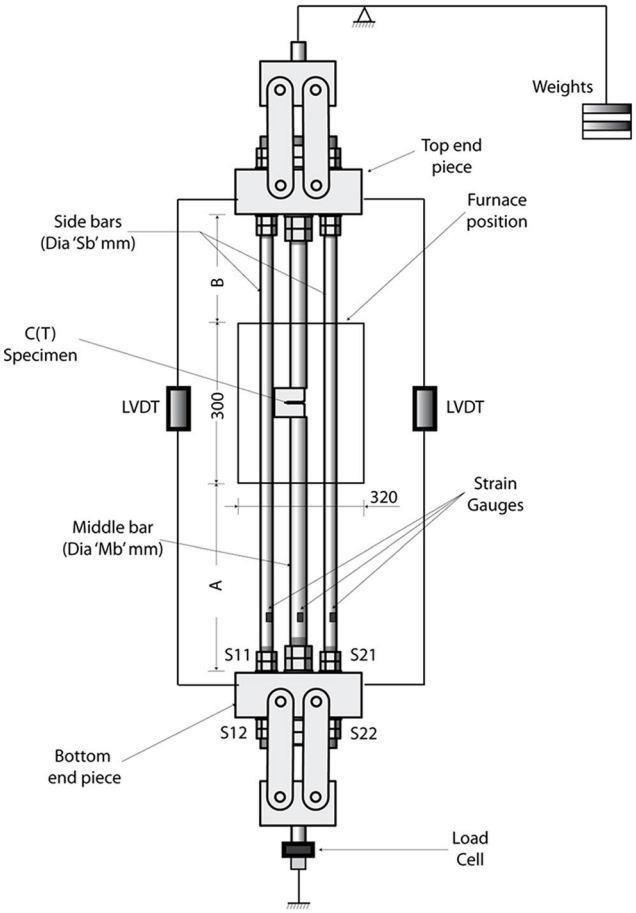

Rig No.	Dimensions (mm)			
	A	B	Sb	Mb
1	312	128	19.62	25.61
2	347	218	10.00	10.00

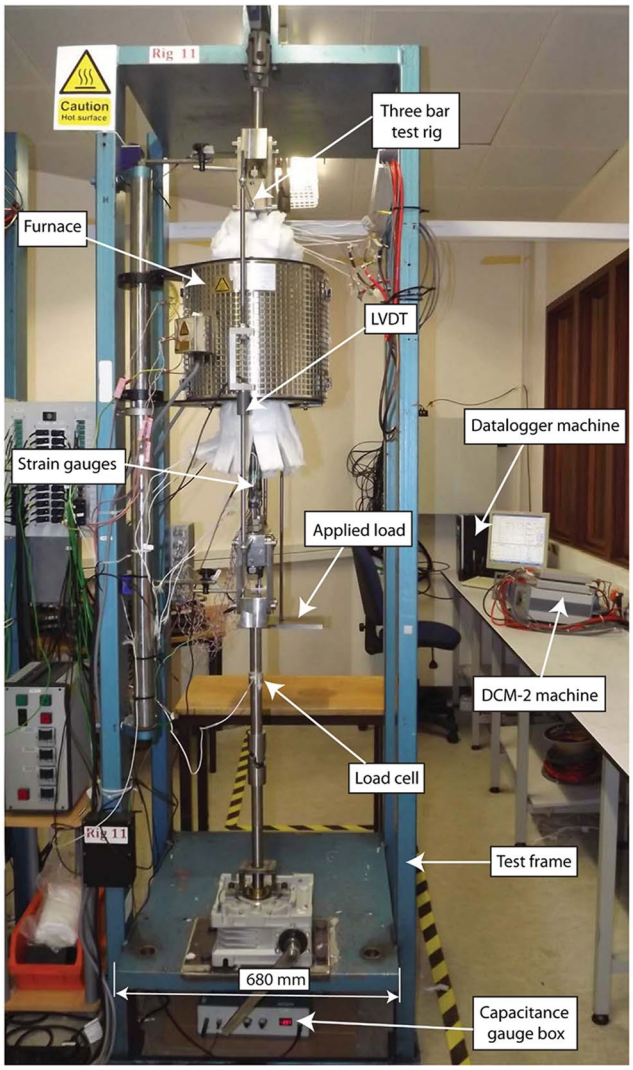

Fig. 5 Creep three-bar test rig (All dimensions in mm)

Table 1 Properties of materials for three-bar structure

Material	Young's modulus (GPa)	Yield strength (0.2% proof stress) (MPa)	Tensile strength (MPa)
316H stainless steel at 550 °C	151	172	444
Nimonic 80A at room temperature	–	875	1210
EN24T steel at room temperature	210	680	925

Table 2 Chemical composition of the 316H stainless steel

Chemical	C	Mn	Si	P	S	Cr	N	Mo	Al	Ti	W	V	Co	Cu
Weight (%)	0.04	1.49	0.29	0.02	0.014	17.1	11	2.38	< 0.005	0.013	0.042	0.02	0.09	0.09

gauge was connected to the C(T) specimen to measure load line displacement. Four high-temperature strain gauges (ZFLA-3-11) were mounted on the middle and side bars at 90^0 intervals around their circumference to measure the applied strains and thus verify the corresponding loads. In total, seven thermocouples were introduced to measure the specimen temperature, room temperature and the temperature at the point of application of strain gauges. A direct current potential drop (PD) system was connected to the C(T) specimen to measure crack initiation and growth. The overall arrangement was fitted into a creep test rig so that an external load was applied to the assembly via a lever arm arrangement as shown in Fig. 5.

Initial designs for the test rigs involved using pins to transfer the load to the C(T) specimen. However, earlier experimental studies by Aird [21] showed that the pin loading introduced significant changes in stiffness due to the presence of localised yielding between the pin and the specimen. To avoid this, screw fittings were introduced in the C(T) specimen and pin loading removed. A schematic of the revised C(T) specimen is shown in Fig. 6.

3 Experimental studies

3.1 Specimen preparation

An ex-service Type 316H stainless steel identified as 2D2/2 (cast no. 55882) was used to manufacture C(T) specimens. The specimens were extracted from thick-walled pipes, so that the cracks were orientated in the axial-radial direction. C(T) specimens were manufactured as per ASTM 1457 [22]

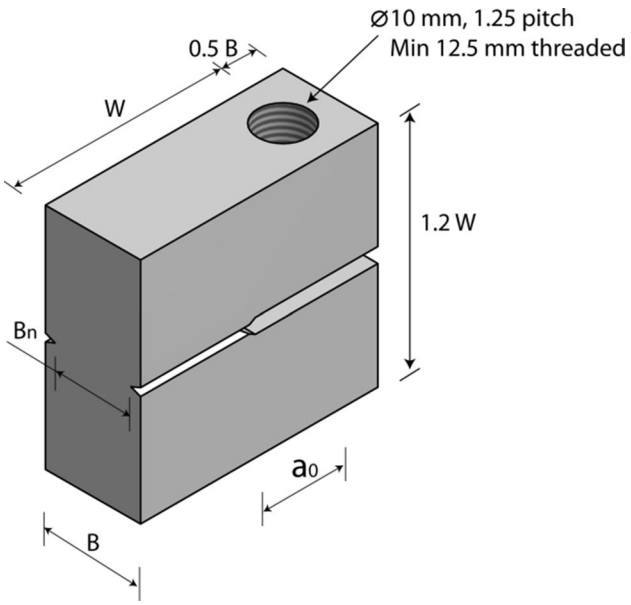

Fig. 6 Screw loaded C(T) specimen

but using a screw fitting arrangement as shown in Fig. 6. This was adopted to ensure accurate measurement of stiffness rather than conventional pin loading. To restrict the crack growth, a 1-mm-diameter hole was introduced at the end of standard 0.1-mm-wide EDM notch. The pre-cracked specimens were then side-grooved each side by 10% of their thickness. The details of the specimens are given Table 3, where W is width, B is gross section thickness, B_n is net section thickness, and a_0 is initial crack length.

3.2 Steps to introduce residual stress into the structure

The residual stress can be introduced into the rig in a controlled manner. This was done by connecting the middle bar with the C(T) specimen to both end pieces. The outer bars were connected to only the top end piece and were free to move through the clearance holes in the bottom end piece. All instruments were then connected to the test rig, and the furnace was heated to achieve 550 °C for the C(T) specimen. This arrangement permitted free thermal expansion of the bars and the specimen. When a stable temperature was achieved, nuts S11 and S21 (shown in Fig. 5) were screwed down, so that the top and bottom end pieces were forced apart. This resulted in the middle bar loaded in tension and the side bars subjected to balancing compressive forces. The force in each bar was determined via the strain gauges. Finally, when the desired residual force was introduced into the structure, nuts S12 and S22 on side bars were fixed. Having introduced the desired residual stress into the C(T) specimen, the entire assembly was then subjected to an applied load. Figure 7 gives the sequence of operation to introduce residual stress. The residual force in all three bars, load line displacement and crack mouth opening displacements (CMOD) of the C(T) specimens, potential drop readings and overall extensions of the rigs were recorded.

3.3 Calibration tests

A series of calibration tests were conducted and divided into two categories; preliminary tests and a load–unload test. Tests were carried out at high temperature and using a 316H stainless steel C(T) specimen. The C(T) specimen was manufactured as per ASTM 1457 [22] but using a screw fitting arrangement rather than pins to load the specimen. This was adopted to ensure accurate measurement of

Table 3 C(T) specimen details

Rig no.	Test ID	W (mm)	B (mm)	B_n (mm)	a_0 (mm)
1 (Low EFU)	MC-01	37.91	19.10	15.46	19.47
2 (High EFU)	MC-02	37.90	19.11	15.46	19.48

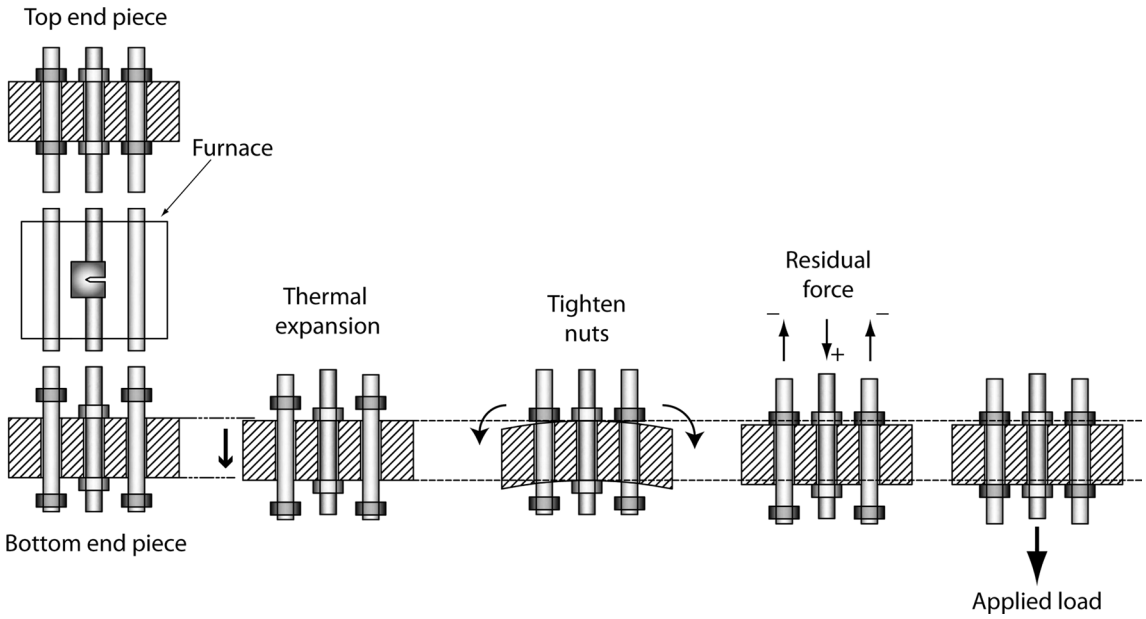

Fig. 7 Sequence of operation at high temperature

stiffness rather than conventional pin loading. To restrict the crack growth, a 1-mm-diameter hole was introduced at the end of standard 0.1-mm-wide EDM notch.

Preliminary tests were conducted to determine the stiffness of bars, specimen and determine the overall elastic follow-up value for the rig experimentally. Two applied load tests, within the elastic region, were conducted such that in each case the temperature of the C(T) specimen was maintained at 550 °C. In the first test, only the middle bar with the C(T) specimen was connected to both end pieces. Then, the furnace was switched on such that the temperature of the C(T) specimen reached 550 °C. When a stable temperature was reached, an external load was applied to the middle bar via a lever arm arrangement. In the second test, both the side bars are connected to the top and bottom end bars, but the middle bar with C(T) specimen was connected only to the top end piece such that it was free to move (i.e. used to record the C(T) specimen temperature). In each case, the load cell, the temperature at different locations, strain gauge, total displacement and CMOD were measured. The results from these tests are discussed later.

The second category of test was a load–unload test undertaken to understand the relaxation of residual force with applied load depending upon the elastic follow-up. First, a residual stress was introduced into the structure as discussed in earlier section. Having introduced the desired residual stress into the C(T) specimen, the entire assembly was repeatedly loaded and unloaded to progressively higher load levels. The residual force in all three bars, load line displacement of C(T) specimen, potential drop readings and overall extension of the rig were recorded for both load and unload path.

4 Results and discussion

4.1 Comparison of theoretical and experimental value of EFU

When the C(T) specimen was maintained at 550 °C, the different sections of the three bars were exposed to different temperatures. The values of temperatures at different locations on the middle and side bars are measured, and a curve was fitted between measured points. Figures 8 and 9 show the temperature distribution in middle and side bars for both rigs, respectively, when C(T) specimen was at 550 °C.

To calculate the theoretical value of EFU, the equations presented in [15] were used. The three-bar structure is further simplified as shown in Fig. 10. The theoretical value of stiffness of C(T) specimen was calculated by using the following equation taken from [23]

$$K_{\text{spec}} = B_n E_{\text{spec}} \left(\frac{1 - a/W}{1 + a/W} \right)^2 \left(\begin{array}{c} 2.163 + 12.219(a/W) - 20.065(a/W)^2 \\ -0.9925(a/W)^3 + 20.609(a/W)^4 \\ -9.9314(a/W)^5 \end{array} \right)^{-1} \quad (3)$$

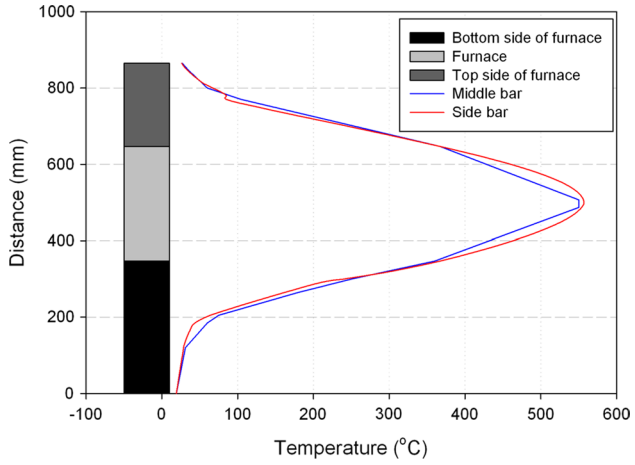

Fig. 8 Temperature distribution in rig 01

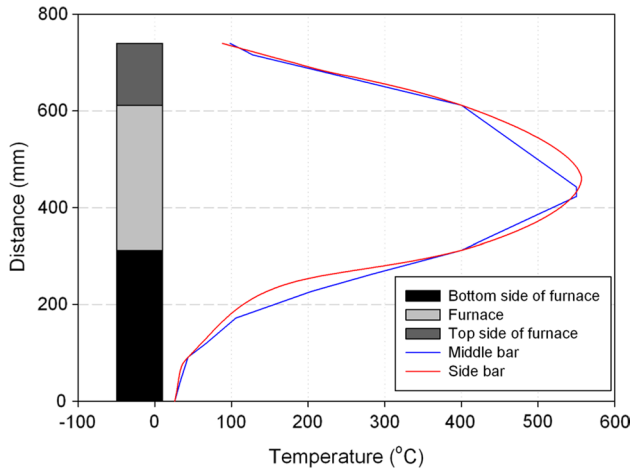

Fig. 9 Temperature distribution in rig 02

where B_n is the thickness of specimen, E_{spec} is the young's modulus, a is the initial crack length, W is the width of the specimen.

For theoretical calculation, an average Young's modulus is taken from Table 4 against the variation of temperature the bar is subjected to. For example, in case of rig no 01, the Nimonic bar 6 (see Fig. 10) was subjected to a temperature variation of 400–543 °C and Young's modulus is calculated by taking the average Young's modulus value for temperature variation of 400–600 °C from Table 4. Theoretical values obtained from analysis are shown in Table 5.

To calculate the experimental value of EFU, data from the preliminary tests performed were used. To find the stiffness of the C(T) specimen, the data from tensile test conducted on middle bar at high temperature were used. The stiffness of the C(T) specimen was calculated using the equation

$$K_{spec} = \frac{\text{Load}}{\text{CMOD}} \tag{4}$$

The stiffness of the middle bar other than specimen is calculated by

$$K_{in} = \frac{\text{Load}}{\text{Total displacement} - \text{CMOD}} \tag{5}$$

Tensile test is conducted on side bar within elastic region at high temperature was used to calculate the stiffness of side bars. Load acting on each bar is calculated using strain gauge mounted and displacement from LVDTs mounted on end pieces.

$$K_{out} = \frac{\text{Load}}{\text{Total displacement}} \tag{6}$$

In both above cases, the total displacement is obtained from LVDT mounted on end pieces.

The experimental EFU and stiffness of components of both rigs are shown in Table 5. A good agreement was found between theoretical and experimental values. The source of error is more where measurement of total displacement over a large length from LVDTs is involved, but this can be improved by using non-contact measurement devices.

4.2 Load–unload tests

The results from the load–unload tests are shown in Figs. 11 and 12 and give the details of variation of the residual force and its relaxation as the applied load increased. It is observed that under equilibrium condition, the total compressive residual force in the side bars was approximately equal to the tensile residual force in middle bar. Tables 6 and 7 show the summary of the tests performed on both rigs.

The reference stress in Table 4 was determined from [24]

$$\sigma_{ref} = \frac{P}{WB_n n_L}, \tag{7}$$

where n_L is a normalised limit load function given by

$$n_L = \sqrt{(1+\gamma)\left(1+\gamma(a/W)^2\right)} - (1+\gamma(a/W)) \quad \text{with } \gamma = 2/\sqrt{3}$$

During the cyclic loading process on rig 01, the tensile residual force in middle bar relaxed from 6.34 kN to 2.84 kN while the average compressive residual force in the side bars relaxed from 3.14 kN and 1.43 kN (see Fig. 11a).

Figure 11b shows the load acting on C(T) specimen against total load line displacement measured during the cyclic loading phase of the test. The following points should be noted. First at point 'A,' the C(T) specimen was subjected to a tensile load of 6.34 kN, while the total load applied to the assembly was zero. This tensile load corresponded to the initial level of preload in the assembly at the start of the cyclic loading phase of the test.

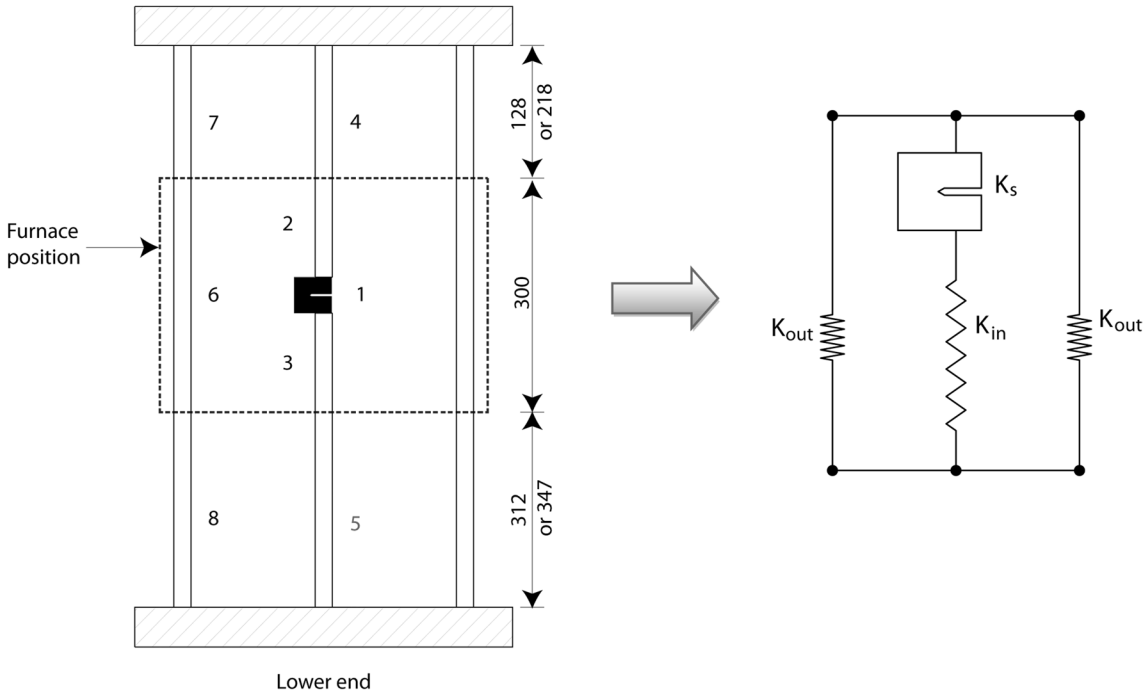

Fig. 10 Simplified three-bar rig for EFU calculation

Table 4 Young's modulus obtained from [special metals]

Temperature (°C)	Rig 01 (GPa)	Rig 02 (GPa)
20	214	222
100	210	219
200	205	213
300	199	208
400	192	201
500	185	194
600	178	188
700	170	180
800	161	170
900	149	159
1000	134	145

Table 5 Comparison of values

	Test rig 01		Test rig 02	
	Theoretical	Experimental	Theoretical	Experimental
K_s (N/mm)	70,322	79,153	70,145	73,826
K_{in} (N/mm)	145,612	104,791	19,924	17,242
K_{out} (N/mm)	79,850	99,582	18,814	17,898
K_{eff} (N/mm)	47,421	45,093	15,516	13,978
β	2.071	1.324	0.284	0.234
α_{eff}	3.368	4.417	2.425	2.561
Z_s	1.483	1.755	4.521	5.282
Z_{eff}	1.297	1.226	1.412	1.390
Z	1.923	2.153	6.385	7.344
$1/Z$	0.520	0.465	0.157	0.136

Second, five unloading lines did not return to the CMOD point 'A' from which the test started. This was due to the accumulation of plastic deformation in the specimen. It can be seen that about 0.06 mm of plastic CMOD had accumulated at the final unloading step. Also, the gradient of each of the unloading lines remained constant. This shows there has been no crack growth during cyclic loading and the same was recorded by PD system. Third, the line AB corresponds to the locus of unloaded points and reveals that the initial preload relaxed, as plastic deformation accumulated in the specimen thereby reducing the misfit. At point B, with an applied load of zero, the 3.14 KN load on the C(T) specimen corresponds to the level of preload remaining in the assembly, i.e. 50% reduction in the initial preload level.

In test on rig 02, the tensile residual force in middle bar relaxed from 6.22 kN to 6.04 kN, while the compressive residual force in the side bars relaxed from 3.09 kN and 2.96 kN (see Fig. 12a). The load acting on C(T) specimen as a function of the total load line displacement measured during the cyclic loading phase of the test is given in Fig. 12b. It is evident from the line AB that corresponds to the locus of unloaded points that no significant relaxation of preload occurred in the second test rig.

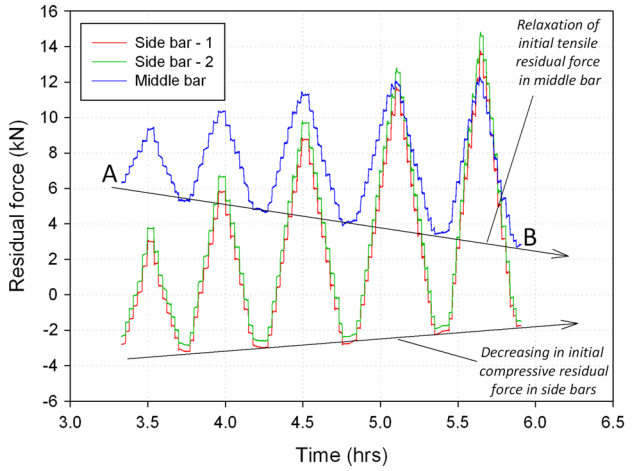

(a) Variation of force in all three bars with time

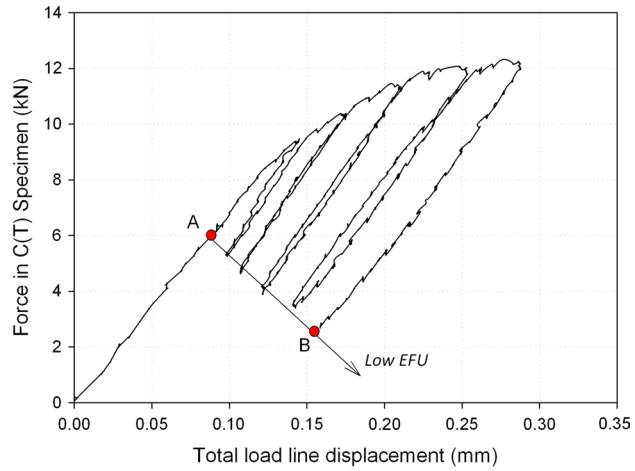

(b) Load versus total load line displacement for C(T) specimen

Fig. 11 Load unload test behaviour on rig 01 at 550 °C

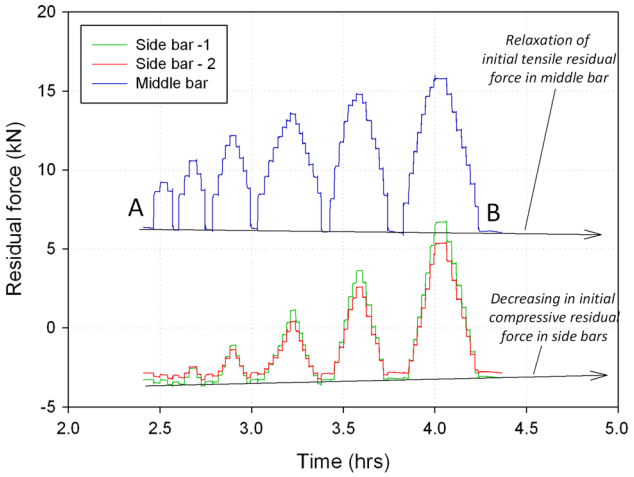

(a) Variation of force in all three bars with time

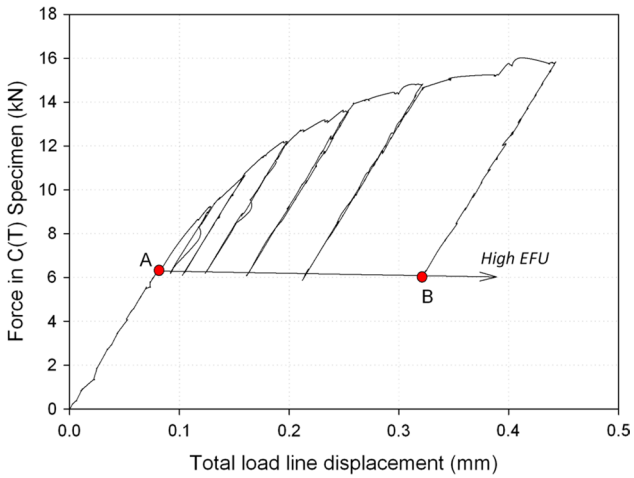

(b) Load versus total load line displacement for C(T) specimen

Fig. 12 Load unload test behaviour on rig 02 at 550 °C

An important feature of the behaviour of both test assembly is that the relaxation line AB has a slope dependent on the relative stiffness of the assembly and in turn corresponded to the EFU associated with the structure. The initial preload relaxes more in rig with low EFU compared to rig with high EFU. The locus of relaxation is linear which shows only C(T) specimen undergoes creep, while others parts behave purely elastic during test period.

4.3 Expected behaviour of the rig for long-term creep tests

Preliminary and load unload tests validated the novel creep test rig designed to carry out mixed boundary tests. In R5, assessment procedure EFU is defined as [20]

$$Z = \frac{\Delta\varepsilon_{\text{Elastic}}}{\Delta\varepsilon_{\text{Creep}}} \tag{8}$$

In R5 standards, the effect of EFU is studied using singe creep component (cantilever beam) and effects of adjacent components in structure are not considered, but practical situation is totally different. If only single component in a structure undergoes creep and remaining components are still in elastic, then it is not addressed in R5.

In newly designed test rig, the reference stress will be equal to induced residual stress plus applied stress. Figure 13 shows the expected behaviour of the three-bar rigs when both rigs are subjected to same initial residual stress and applied stress. If only C(T) specimen creeps and other parts of the structure are still in elastic, the relaxation curve will be linear and will depend upon EFU following either path AC or AD. If components other than C(T) specimen also creep in structure, the relaxation curve will follow nonlinear path AE. The rate of relaxation of total

Table 6 Summary of load unload test on rig 01 (low EFU)

	Side bar-1	Side bar-2	Middle bar	Specimen
I[a]				
Avg strain (×E-6)	−53.76	−47.10	59.17	–
Residual force (N)	−3.345	−2.939	6.339	6.339
Residual/reference stress (MPa)	−11.07	−9.70	12.31	129.37
II[b]				
Avg strain (×E-6)	−23.35	−22.28	26.51	–
Residual force (N)	−1.462	−1.395	2.839	2.839
Residual/reference stress (MPa)	−4.84	−4.61	5.51	57.95

[a]After inducing residual force

[b]At the end of load–unload test

Table 7 Summary of load–unload test on rig 02 (high EFU)

	Side bar-1	Side bar-2	Middle bar	Specimen
I[a]				
Avg strain (×E-6)	−182.07	−172.31	356.84	–
Residual force (N)	−3.175	−3.005	6.222	6.222
Residual/reference stress (MPa)	−40.41	−38.25	79.22	127.32
II[b]				
Avg strain (×E-6)	−176.80	−163.13	346.22	–
Residual force (N)	−3.083	−2.844	6.037	6.037
Residual/reference stress (MPa)	−39.25	−36.22	76.86	123.53

[a]After inducing residual force

[b]At the end of load unload test

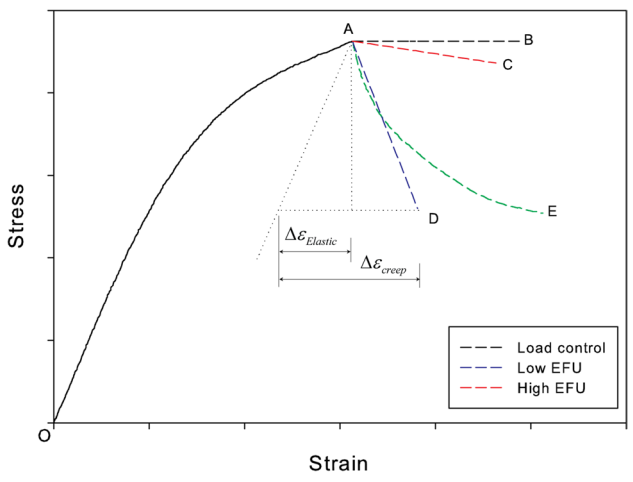

Fig. 13 Expected behaviour of long-term creep tests

residual stress due to thermal ageing and crack growth will be lower in rig with high EFU compared to low EFU rig. This relaxation will also increase the crack initiation time when compared to the load control tests. More details about the long-term tests are given in [25].

5 Concluding remarks

Four methods of inducing residual stress in laboratory creep specimens were reviewed. These include quenching, side punching, in-plane compression and welding methods. It was found that the ability of these methods to provide insight into the effect of residual stress on creep in engineering structures is limited. These methods cause microstructural changes to the material as well as inducing residual stress. Also, the short-range residual stresses produced by some of the methods do not accurately represent the long-range residual stresses found in many engineering structures. In each of these methods, residual stress measured at room temperature before the start of test will change when the specimen is subjected to high temperature. None of the methods determine the effect of residual stress on creep and complete structure when the residual stress relaxes. We therefore conclude that new methods which can induce long-range residual stress without causing microstructural change in the material and can represent combined boundary condition are required.

A new method based on a three-bar structure illustrated that residual stresses can be induced into a specimen at high temperature in a controlled manner and can

be characterised easily without the use of time-consuming measurement techniques. The proposed method does not cause any microstructural change in the specimen and provides details of residual stresses distribution in complete structure at any time. Calibration tests revealed that the structure replicates mixed boundary conditions present in practical situation. Different combinations of diameters of the middle and side bars can be used to achieve different elastic follow-up factors and can therefore study the influence of EFU on initial residual stress and structure as a whole. Experimental tests revealed that the initially induced residual force relaxed at a rate governed by the elastic follow-up provided by the test rigs. In line with this, if long-term creep tests are carried out [say on C(T) specimen] using the rig and compared with the same initial reference stress load-controlled test, the initiation times for the combined residual and applied loads will be longer, with increasing initiation times for lower values of elastic follow-up. The longer initiation times are a consequence of the relaxation and redistribution of the residual loads in the rigs. The new method and the test rig designed can be used for both cracked and uncracked specimens to carry out short- and long-term creep tests.

Acknowledgements The authors gratefully acknowledge EDF Energy for providing financial support for this work. David Smith is also supported by the Royal Academy of Engineering, EDF-Energy and Rolls-Royce plc.

References

1. Kapadia P, Davies CM, Dean DW, Nikbin KM (2012) Numerical simulation of residual stresses induced in compact tension specimens using electron beam welding. In: Proceedings of the ASME 2012 pressure vessels and piping conference, 15–19 July 2012, Toronto, ON, Canada
2. Aird CJ, Mahmoudi AH, Mirzaee Sisan A, Truman CE, Smith DJ (2006) Generating well defined residual stresses in laboratory specimens. In: Proceedings of the ASME 2006 pressure vessels and piping conference, 23–27 July 2006, Vancouver, BC, Canada
3. Turski M (2004) High temperature creep cavitation cracking under the action of residual stress in 316H stainless steel. PhD thesis, University of Manchester, UK
4. O'Dowd NP, Nikbin KM, Wimpory RC, Biglari FR, O'Donnell MP (2008) Computational and experimental studies of high temperature crack initiation in the presence of residual stress. J Press Vessel Technol 130:0414031–0414037
5. O'Dowd NP, Nikbin KM, Wimpory RC, Biglari FR (2005) Creep crack initiation in a weld steels: effects of residual stress. In: Proceedings of pressure vessels and piping conference, PVP2005, 17–21 July 2005, Denver, CO, USA
6. Kamel S, Davies C, Lee H, Nikbin K (2010) Effect of crack extension in a compact tension C(T) specimen containing a residual stress on the stress intensity factors. In Proceedings of the ASME 2010 pressure vessels and piping conference, PVP2010, 18–22 July 2010, Bellevue, Washington, USA
7. Nezhad HY, O'Dowd NP, Davies CM, Nikbin KM, Wimpory RC (2011) Study of creep relaxation behaviour of 316 h austenitic steels under mechanically induced residual stress. In: Proceedings of the ASME 2011 pressure vessels and piping conference, PVP2011, 17–21 July 2011, Baltimore, MD, USA
8. Hossain S (2005) Residual stresses under conditions of high triaxiality. PhD thesis, University of Bristol, UK
9. Hossain S, Truman CE, Smith DJ (2011) Generation of residual stress and plastic strain in a fracture mechanics specimen to study the formation of creep damage in type 316 stainless steel. Fatigue Fract Eng Mater Struct 34:654–666
10. Spindler MW (2000) The use of borland specimens to reproduce reheat cracking in type 316H. Technical report, British Energy Generation Ltd., Report No. EPD/AGR/REP/0618/99 Issue 1, Feb 2000
11. Dennis RJ (2008) Detailed analysis of ring-weld creep test specimen. Technical report, British Energy Generation Ltd., Report No. BBGB/007/01 Issue 1, Feb 2008
12. Davies CM, Wimpory RC, Dean DW, Webster G, Nikbin KM (2007) Effect of residual stresses on crack growth in 316 h steel weldments. In: 3rd international conference on integrity of high temperature welds, pp 333–344, 24–26 April 2007
13. Davies CM, Hughes D, Wimpory RC, Dean DW, Nikbin KM (2010) Measurements of residual stresses in 316 stainless steel weldments. In: Proceedings of the ASME 2010 pressure vessels and piping conference, PVP2010, 18–22 July 2010, Bellevue, Washington, USA
14. Hadidi-Moud S, Smith DJ (2008) Use of elastic follow-up in integrity assessment of structures. In: Proceedings of the ASME 2008 pressure vessels and piping conference, 27–31 July 2008, Chicago, IL, USA
15. Smith DJ, McFadden J, Hadidimoud S, Smith AJ, Stormonth Darling AJ, Aziz AA (2010) Elastic follow-up and relaxation of residual stresses. Proc Inst Mech Eng Part C J Mech Eng Sci 224:777–787
16. Robinson EL (1955) Steam piping design to minimize creep concentration. Trans ASME 77:1147–1162
17. Boyle JT, Nakamura K (1987) The assessment of elastic follow-up in high temperature piping systems—overall survey and theoretical aspects. Int J Press Vessels Pip 29:167–194
18. Kobayashi K, Abe S, Udoguchi T (1986) Stress and strain behaviour under uniaxial elastic follow-up. Bull JSME 257:3672–3678
19. Kasahara N, Nagata T, Iwata K, Negishi H (1995) Advanced creep–fatigue evaluation rule for fast breeder reactor components: generalization of elastic follow-up model. Nucl Eng Des 155:499–518
20. British Energy Generation Ltd. (2003) Assessment procedure for the high temperature response of structures. R5, Issue 3
21. Aird CJ (2009) The influence of long-range residual stress on the cleavage fracture of ferritic steel. PhD thesis, University of Bristol
22. American Society for Testing and Materials (2000) Standard test method for measurement of creep crack growth rates in metals. ASTM E1457-00
23. Anderson TL (2005) Fracture mechanics—fundamentals and applications. Taylor and Francis, New York
24. R6 Revision 4 Amendment 8 (2010) Assessment of the integrity of structures containing defects. BEGL procedure
25. Shirahatti AM, Truman CE, Smith DJ (2013) Experiments to determine the influence of residual stress and elastic follow-up on creep crack initiation. In: Proceedings of the ASME 2013 pressure vessels and piping conference, 14–18 July 2013, Paris, France